

1 **Climatic variations during the Holocene inferred from**
2 **radiocarbon and stable carbon isotopes in speleothems from a**
3 **high-alpine cave**

4 Caroline Welte^{1,2}, Jens Fohlmeister^{3,4}, Melina Wertnik^{1,2}, Lukas Wacker¹, Bodo Hattendorf⁵,
5 Timothy I. Eglinton², Christoph Spötl⁶

6 ¹ Laboratory of Ion Beam Physics, ETHZ, Otto-Stern Weg 5, 8093 Zurich, Switzerland,

7 ² Geological Institute, ETHZ, Sonnegstrasse 5, 8092 Zurich, Switzerland

8 ³ Potsdam Institute for Climate Impact Research, Telegrafenberg, 14473 Potsdam, Germany

9 ⁴ GFZ German Research Centre for Geosciences, Section 'Climate Dynamics and Landscape Development', 14473
10 Potsdam, Germany

11 ⁵ Laboratory of Inorganic Chemistry, D-CHAB, ETHZ, Vladimir-Prelog Weg 1, 8093 Zurich, Switzerland

12 ⁶ Institute of Geology, University of Innsbruck, Innrain 52f, 6020 Innsbruck, Austria

13

14 Keywords: radiocarbon, stable carbon isotopes, LA-AMS, speleothems, high-alpine cave

15 *Correspondence to:* Caroline Welte: cwelte@phys.ethz.ch, Jens Fohlmeister: jens.fohlmeister@pik-potsdam.de

16

17

18 **Abstract**

19 Rapid and continuous analysis of radiocarbon (^{14}C) concentration in carbonate samples at spatial resolution down
20 to 100 μm has been made possible with the new LA-AMS (laser ablation accelerator mass spectrometry)
21 technique. This novel approach can provide radiocarbon data at a spatial resolution similar to that of stable carbon
22 (C) isotope measurements by isotope ratio mass spectrometry of micromilled samples and, thus, can help to
23 interpret $\delta^{13}\text{C}$ signatures, which otherwise are difficult to understand due to numerous processes contributing to
24 changes in C-isotope ratio. In this work, we analyzed $\delta^{13}\text{C}$ and ^{14}C on the Holocene stalagmite SPA 127 from the
25 high-alpine Spannagel Cave (Austria). Both proxies respond in a complex manner to climate variability. Combined
26 stable carbon and radiocarbon profiles allow to identify three growth periods characterized by different $\delta^{13}\text{C}$
27 signatures: (i) the period 8.5 to 8.0 ka BP is characterized by relatively low $\delta^{13}\text{C}$ values with small variability
28 combined with a comparably high radiocarbon reservoir effect (expressed as dead carbon fraction, dcf) of around
29 60%. This points towards C contributions of host rock dissolution and/or from an “old” organic matter (OM)
30 reservoir in the karst potentially mobilized due to the warm climatic conditions of the early Holocene. (ii) Between
31 8 and 3.8 ka BP a strong variability in $\delta^{13}\text{C}$ with values ranging from -8 to +1‰ and a generally lower dcf. The
32 $\delta^{13}\text{C}$ variability is most likely caused by changes in C exchange between cave air CO_2 and dissolved inorganic
33 carbon in drip water in the cave, which are induced by reduced drip rates as derived from reduced stalagmite
34 growth rates. Additionally, the lower dcf indicates that the OM reservoir contributed less to stalagmite growth in
35 this period possibly as a result of reduced meteoric precipitation or because it was exhausted. (iii) In the youngest
36 section between 3.8 and 2.4 ka BP, comparably stable and low $\delta^{13}\text{C}$ values combined with an increasing dcf
37 reaching up to 50% again hint towards a contribution of an aged OM reservoir in the karst. This study reveals the
38 potential of combining high-resolution ^{14}C profiles in speleothems with $\delta^{13}\text{C}$ records in order to disentangle
39 climate-related C dynamics in karst systems.

40 **1 Introduction**

41 Understanding the climate of the past is the key for understanding how climate and environment will change in
42 the future. Insights into paleoclimate are gained through the study of archives with stalagmites being a prominent
43 example for a terrestrial archive. Stalagmites can grow continuously over thousands to tens of thousands of years
44 (Cheng et al., 2016; Fairchild et al., 2006; Moseley et al., 2020). Caves hosting stalagmites are present on all
45 continents except Antarctica and uranium-series disequilibrium dating allows to build robust chronologies (Cheng
46 et al., 2013; Richards and Dorale, 2003; Scholz and Hoffmann, 2008). Trace-element and stable isotope data of
47 stalagmites allow the reconstruction of climatic conditions in the past. For example, the oxygen isotope
48 composition ($\delta^{18}\text{O}$) is generally interpreted as a combination of a temperature and a meteoric precipitation signal
49 (Lachniet, 2009; Wackerbarth et al., 2010). The interpretation of the stable carbon isotope signature ($\delta^{13}\text{C}$),
50 however, is more challenging since additional local effects, such as vegetation changes (e.g., Bar-Matthews et al.,
51 1999; Denniston et al., 2007; Fohlmeister et al., 2020), the carbonate dissolution mechanism (e.g., Fohlmeister et
52 al., 2010b; Lechleitner et al., 2016), and in-cave fractionation processes (e.g., Matthey et al., 2016; Spotl et al.,
53 2005) may have an influence and little is known about the relative magnitude of these processes. Besides the stable
54 C isotopes, radiocarbon (^{14}C), decaying with a half-life of ~ 5700 yrs (Kutschera, 2013), can be a valuable tool in
55 speleothem research (e.g., Bajo et al., 2017; Lechleitner et al., 2016). So far, this isotope has not been fully
56 exploited in speleothem science, mostly due to the time-consuming sampling and processing as well as the
57 comparably high costs associated with the analyses. However, recently both issues have been considerably

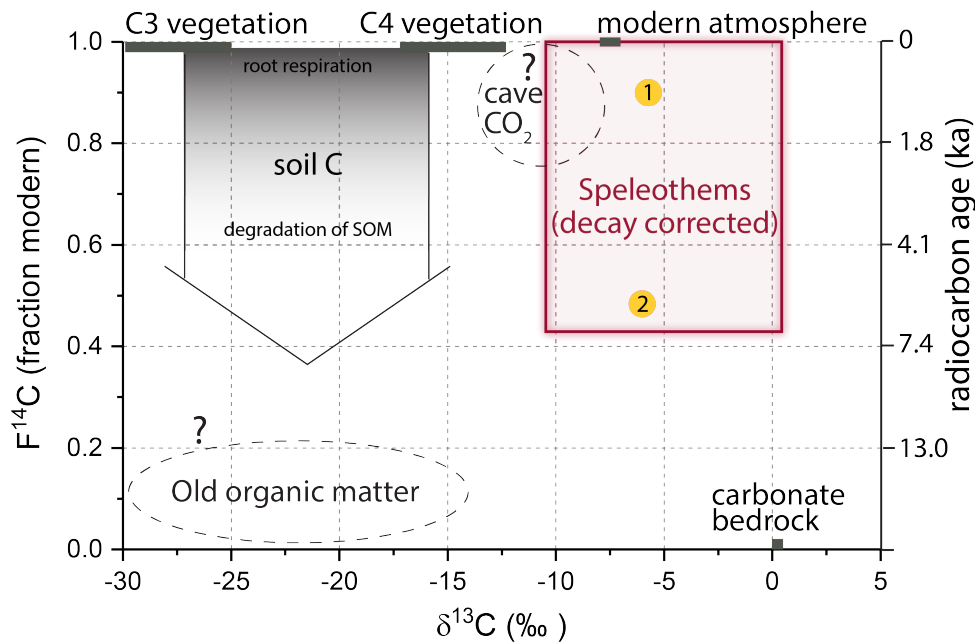
58 improved by invention (Welte et al., 2016a; Welte et al., 2016b) and advances in laser ablation coupled to
59 accelerator mass spectrometry (LA-AMS; Welte et al., 2017; Yeman et al., 2019), which can be well applied to
60 carbonate material.

61 We investigated a stalagmite that grew in the Spannagel cave system (Tyrol, Austria; Spötl et al., 2004) by means
62 of C isotope systematics. This high-alpine cave system was investigated in many studies in the context of
63 palaeoclimate and palaeoenvironmental research mostly using O isotopes and growth phases as proxies (e.g.,
64 Fohlmeister et al., 2013; Spötl and Mangini, 2010). The gneiss covering the cave-bearing marble contains
65 interspersed fine-crystalline pyrite (Spötl et al., 2004) and is topped by a thin soil layer with sparse vegetation. It
66 was hypothesized that the oxidation of pyrite contributes considerably to the dissolution of the host-rock marble
67 and, hence, to the growth of stalagmites and flowstones, in particular during cold climate periods when there is no
68 soil present at this high altitude (Spötl and Mangini, 2007). During some interglacials including the Holocene,
69 when Alpine soils are present in the catchment of the cave's drip water, sulfide oxidation and soil-derived CO₂
70 may operate in tandem. Consequently, the stable C isotope signal of stalagmites from this cave is expected to vary
71 significantly.

72 The aim of this study is to gain deeper insights into the climatically driven C dynamics in this cave by high spatially
73 resolved ¹⁴C analyses of a Holocene stalagmite. This study takes advantage of the recently introduced method of
74 LA-AMS (Welte et al., 2016a; Welte et al., 2016b), which reaches a similar spatial resolution as micro-milling for
75 stable isotope analysis (e.g., Spötl and Matthey, 2006). Using the combined ¹⁴C and δ¹³C records measured in this
76 study as well as the previously published δ¹⁸O signal (Fohlmeister et al., 2013), we explore the key processes
77 influencing the carbon isotope composition of speleothems in this cave and gain a better understanding of the
78 potential and limits of ¹⁴C analysis of carbonates using LA-AMS.

79 **2 Radiocarbon and dead carbon fraction**

80 In most karst systems, dissolution of the carbonate host rock is driven by soil-derived carbonic acid forming in
81 meteoric precipitation seeping through the soil. In this case, the two major soil-derived C sources contributing to
82 the δ¹³C values of the speleothem are pedogenic CO₂ from the degradation of soil organic matter (SOM, Trumbore,
83 2000) and root respiration (Cerling, 1984) that acidifies the meteoric water as it percolates through the soil.
84 Recently, evidence was found for a potential additional C source stemming from CO₂ derived from the oxidation
85 of "old" organic matter (OM) in the deep vadose zone (Bergel et al., 2017; Noronha et al., 2015). The water
86 charged with carbonic acid then dissolves the host rock CaCO₃. In some karst systems, the oxidation of pyrite has
87 shown to contribute to the acidification of the seepage water and hence to speleothem formation (e.g., Spötl et al.,
88 2016). All of those C-pools have different characteristics with respect to their stable and radioactive isotope
89 signatures (Fig. 1).



90

91 *Figure 1: Carbon isotopic signatures of carbon-bearing reservoirs in karst systems. Yellow circles mark speleothem-C resulting*
 92 *from different processes: 1. CaCO₃ dissolution via soil CO₂-derived carbonic acid. 2. Deep organic carbon contribution to*
 93 *seepage water feeding speleothems (adapted from Fairchild and Baker (2012)).*

94 When working with radiocarbon in speleothems it is important to determine the reservoir effect (Genty and
 95 Massault, 1997). If a radiocarbon-independent chronology for the stalagmite exists, the reservoir effect, which is
 96 often termed dead carbon fraction (dcf), can be derived through comparison of the measured ¹⁴C profile in the
 97 stalagmite ($F^{14}C_{stal}$) with the ¹⁴C atmosphere's signature ($F^{14}C_{atm}$) of the same time (Genty and Massault (1997)):

98
$$dcf = \left(1 - \frac{F^{14}C_{stal}}{F^{14}C_{atm}}\right) \cdot 100\% \quad (1)$$

99 Values for dcf range from a few % up to 70% (Bajo et al., 2017; Southon et al., 2012) and commonly vary within
 100 a single speleothem with time (Bajo et al., 2017; Noronha et al., 2014; Therre et al., 2020). The magnitude of the
 101 dcf is influenced by multiple factors, such as the age of soil OM, contributing to soil gas CO₂ production
 102 (Fohlmeister et al., 2011b) and consequently altering the ¹⁴C concentration in the stalagmite. Also the CO₂ partial
 103 pressure (pCO₂) in the soil plays an important role, with a complex relationship between the amount of soil gas
 104 pCO₂ and the dcf (Fohlmeister et al., 2011b). Additionally, the conditions of karst dissolution, i.e. open vs. closed
 105 system (Fohlmeister et al., 2011a; Hendy, 1971), affect the dcf. In a more open system, the dcf is low because the
 106 percolating water can continuously exchange C isotopes with the soil gas CO₂ leading to a ¹⁴C concentration in
 107 the stalagmite that is dominated by the near-atmospheric soil ¹⁴C signature (Southon et al., 2012). In a more closed
 108 system, this exchange is inhibited with the extreme case being a completely closed system, where for each mole
 109 of carbonic acid one mole of CaCO₃ is dissolved resulting in a dcf of up to 50% (Hendy, 1971). Fractionation and
 110 C exchange between cave air CO₂ and dissolved inorganic carbon (DIC) in drip water are also potential candidates
 111 for modulation of the dcf. These main factors driving the dcf in turn are influenced by numerous parameters such
 112 as hydrological and environmental conditions above the cave. Several studies (e.g., Bajo et al., 2017; Fohlmeister
 113 et al., 2010a; Griffiths et al., 2012; Lechleitner et al., 2016; Noronha et al., 2014) showed that during periods of
 114 increased rainfall the dcf in the stalagmite is enhanced. A likely explanation is a shift towards more closed-system
 115 conditions (Table 1) under higher meteoric precipitation regimes. It was argued, that under more humid (arid)

116 conditions the pore spaces in soils are clogged with (devoid of) water, leaving less (more) opportunity for C-
 117 exchange processes between dissolved inorganic C species and soil gas CO₂ (Fohlmeister et al., 2010).

118 An increasing number of cave systems have been reported where carbonate dissolution occurs even if no
 119 significant soil exists above the cave, indicating climatic conditions less suited for the existence of vegetation
 120 cover. Acidic conditions in the seepage water are achieved via oxidation of pyrite or other sulfide minerals
 121 disseminated in the bedrock (Bajo et al., 2017; Lauritzen, 2001; Spötl et al., 2016). In this case the C isotope
 122 composition in the drip water is dominated by the bedrock, and the dcf is therefore expected to be relatively high
 123 (>50%). Under those conditions the δ¹³C values of the speleothems reflect those of the (marine-derived) bedrock,
 124 i.e. are shifted closer to 0‰ compared to lower δ¹³C values of speleothem CaCO₃ of around -12 to -10‰ for cave
 125 systems with a soil and vegetation cover. An overview of relevant processes as well as the resulting dcf and δ¹³C
 126 are summarized in Table 1.

127 *Table 1 Simplified summary of expected δ¹³C (assuming C3 vegetation cover) and dcf values in stalagmite CaCO₃ for*
 128 *different dominant processes. In many karst systems various combinations of these processes complicate the interpretation.*
 129 *This table is a compilation of data from Fohlmeister et al. (2011b); Spötl et al. (2016); Therre et al. (2020)*

Process		Expected δ ¹³ C (‰)	Expected dcf (%)
Carbonate dissolution via carbonic acid	open-system	< -10‰	Comparably low, i.e. around 10%
	closed-system	> -10‰	Comparably high, i.e. close to 50%
Carbonate dissolution via oxidation of pyrite		Close to 0‰	Very high, i.e. > 50%
“Old” OM contribution to seepage water acidification		< -10‰	Shift towards higher values (> 50% possible)

130

131 3 Materials & Methods

132 3.1 Sample

133 Spannagel cave is located in the Tux Valley (47.08028°N, 11.67167°E; Zillertal Alps, western Austria) and opens
 134 at 2531 m above sea level. It forms a more than 12 km-long system of galleries and short shafts, which developed
 135 in a Jurassic marble tectonically overlain by gneiss. This superposition does not only allow for high-precision U-
 136 series dating of stalagmites due to their relatively high U contents, but also gives rise to carbonate dissolution via
 137 sulfuric acid stemming from pyrite oxidation. The thin alpine soil provides an additional pedogenic source of
 138 acidity and the interplay between the two processes is reflected by highly variable stable C isotope values as well
 139 as dcf in Spannagel speleothems. Stalagmite SPA 127 was found in the eastern part of the cave system, which was
 140 never ice-covered during the Holocene (Fohlmeister et al., 2013). The stalagmite grew from 8.45 to 2.24 ka BP
 141 with an average growth rate of 25 μm/a based on nine U/Th-ages (Fohlmeister et al., 2013). There is no macro-
 142 and microscopic evidence for the existence of hiatuses in this specimen. Further evidence for the absence of
 143 hiatuses is provided by two additional speleothems, SPA 12 and SPA 128, from the same cave are partly coeval
 144 with SPA 127. These additional speleothems have a higher dating density in parts, where SPA 127 has only a few
 145 radiometric U-Th dating points and also do not show evidence of hiatuses (Fohlmeister et al., 2013). In

146 combination with the well replicated stable O isotope signals we are confident that the growth of SPA 127 was not
147 interrupted by hiatuses.

148 The 15 cm-long polished slab of the stalagmite analyzed in this study was first used for stable oxygen and carbon
149 isotope analysis where sampling was performed along the extension axis. For LA-AMS analysis, the same section
150 was used but broken in two pieces at a distance from top (dft) of approximately 10 cm, which will be referred to
151 as “top piece” and “bottom piece”.

152 1. Stable isotope analysis

153 Subsamples for stable carbon isotope analysis were micromilled at 100 μm increments and measured using an
154 automated online carbonate preparation system linked to a triple collector gas source mass spectrometer
155 (Delta^{plus}XL, ThermoFisher, Bremen, Germany) at the University of Innsbruck. Values are reported relative to the
156 Vienna Pee Dee Belemnite standard. The long-term precision of the $\delta^{13}\text{C}$ values (1 standard deviation of replicate
157 analyses) is 0.06‰ (Spötl, 2011). The respective $\delta^{18}\text{O}$ values have been published earlier (Fohlmeister et al., 2013).

158

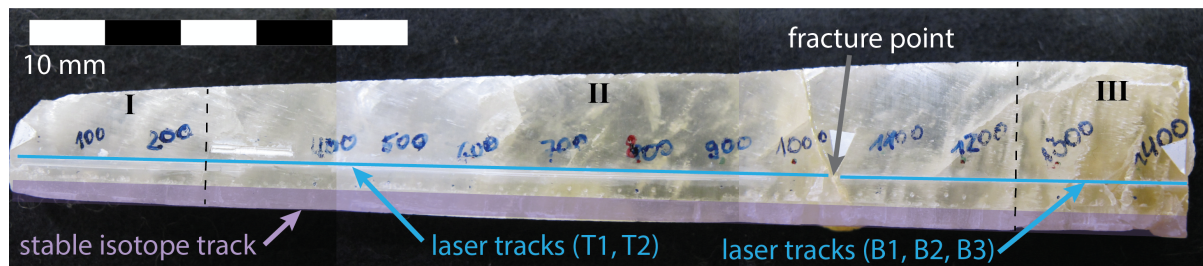
159 3.2 Radiocarbon analysis using LA-AMS

160 By focusing a laser on the surface of a solid sample at sufficiently high energy densities, a small portion of material
161 is ablated and can be used for trace element or isotopic analysis allowing for fast and spatially resolved analysis
162 (Gray, 1985; Koch and Gunther, 2011). ^{14}C analysis of SPA 127 was performed at the Laboratory of Ion Beam
163 Physics, ETH Zurich, Switzerland, by LA coupled with AMS (Welte et al., 2016a; Welte et al., 2017). For this
164 study, a slightly modified LA-AMS setup was used reaching a smaller spot size ($75 \times 140 \mu\text{m}^2$) and higher energy
165 densities of up to 8 J/cm^2 allowing for increased signal intensities, i.e. ^{12}C -currents. With LA-AMS a quasi-
166 continuous data stream is produced at 10 sec intervals in the AMS. This is the minimal integration time of the
167 AMS and together with the laser spot width d and the scanning velocity v defines the spatial resolution R according
168 to $R = d + v \cdot 10 \text{ sec}$.

169 LA-scans were placed as close as possible to the stable isotope tracks in order to facilitate matching between the
170 two data sets (Fig. 2). However, the LA-AMS setup does not permit to place laser tracks close to the rim of samples
171 causing an offset between the two sampling lanes of approximately 5 mm. Speleothem growth layers are often
172 curved, resulting in a potential offset between stable isotope and radiocarbon data of up to several hundred
173 micrometers, with the outer LA-scan appearing somewhat older than the stable isotope record. Since the curvature
174 of the growth layers is most likely variable, a constant correction factor has not been applied.

175 On the “top piece” of SPA 127 two subsequent scans in opposite direction were performed, first from young to
176 old (T1) and then vice versa (T2) on the same track with a scanning velocity of $20 \mu\text{m/s}$ and a laser energy density
177 of approximately 5 J/cm^2 . On the “bottom piece” a total of three analyses were performed: the initial scan from
178 old to young (B1: $10 \mu\text{m/s}$, $1\text{-}2 \text{ J/cm}^2$) was followed by a second repeated scan from bottom to top (B2: old to
179 young, $25 \mu\text{m/s}$, 8 J/cm^2) after removing the top $\sim 0.5 \text{ mm}$ of the sample surface by mechanical polishing. The
180 second scan was necessary to ensure that the unusual ^{14}C signature observed in the oldest part of the stalagmite
181 during the first scan (see section 4) was not the result of a potentially contaminated surface. A final third analysis
182 (B3) consisting of two scans performed in opposite directions was performed at $20 \mu\text{m/s}$ and 5 J/cm^2 . Processing
183 of the raw ^{14}C data was performed using in-house standards also analyzed by LA-AMS for blank subtraction and
184 standard normalization (marble, $F^{14}\text{C} = 0$ and coral standard, $F^{14}\text{C} = 0.9445 \pm 0.0018$) and a conventional
185 fractionation correction to a $\delta^{13}\text{C}$ of -25‰ was applied (Stuiver and Polach, 1977). A Savitzky-Golay (SG) filter
186 is applied to the recorded ^{14}C signal of B3, which is a smoothing method that reduces noise while maintaining the

187 shape and height of peaks (Savitzky and Golay, 1964). In brief, a polynomial is fitted to a sub-set of the data points
 188 and evaluated at the center of the approximation interval. Two parameters, namely the number of points defining
 189 the approximation interval and the maximum polynomial order, can be defined. The smoothing has been applied
 190 to the two sub-scans of B3 (from “old to young” and vice versa) as well as to the combined data to ensure
 191 robustness of the filter. Corresponding uncertainties are estimated from the square root of the sum of the squared
 192 difference between the measured $F^{14}C$ value and the SG fit at each point within the interval. This value is then
 193 divided by the square root of the difference between the interval length (number of data points) and the maximum
 194 order allowed for the polynomial, which is equivalent to the degree of freedom.



195
 196 *Figure 2: Polished slab of SPA 127 (top is left). The locations of the stable isotope track and of the LA-AMS tracks are marked*
 197 *in purple and blue, respectively. The total length of the slab is 14.6 cm. Roman numbers and dashed black lines mark the three*
 198 *sections discussed separately.*

199 4 Results

200 4.1 Dead carbon fraction

201 ^{14}C results for both pieces of SPA 127 (T1, T2 and B3) are reported as dcf (blue line in Fig. 3 a and Fig. S8 a).
 202 Using the ^{14}C profile of the speleothem, the StalAge (Scholz and Hoffmann, 2011) age-depth model applied to
 203 previously published U-Th data (Fohlmeister et al., 2013) and the known ^{14}C content of the atmosphere during the
 204 Holocene (Reimer et al., 2016), the dcf was calculated according to equation (1) for the 1402 radiocarbon data
 205 points (Fig. 3 a). A Savitzky-Golay (SG) filter was applied (interval: 21, maximum polynomial order: 2) and for
 206 comparison the $\delta^{18}O$ and $\delta^{13}C$ data are shown in the same graph (Fig. 3 a and b). The U-Th-dates and the
 207 corresponding average growth rate calculated using StalAge are displayed in Fig. 4 c.

208 4.2 Stable C isotopes

209 The previously published $\delta^{18}O$ values (Fohlmeister et al., 2013) and unpublished $\delta^{13}C$ data (this study) are shown
 210 in Fig. 3 a and b, respectively. A large amplitude and fast changes ranging from -8‰ to +1‰ characterize $\delta^{13}C$
 211 throughout the entire length of the speleothem but are especially pronounced between 30 and 130 mm (ca. 4.0-
 212 8.1 ka BP). Layers exhibiting a comparably stable $\delta^{13}C$ occur at the top and bottom of SPA 127, specifically
 213 ranging from 4 to 25 mm (ca. 2.6 and 3.7 ka BP) and from 130 to 144 mm (ca. 8.1-8.4 ka BP).

214 5 Discussion

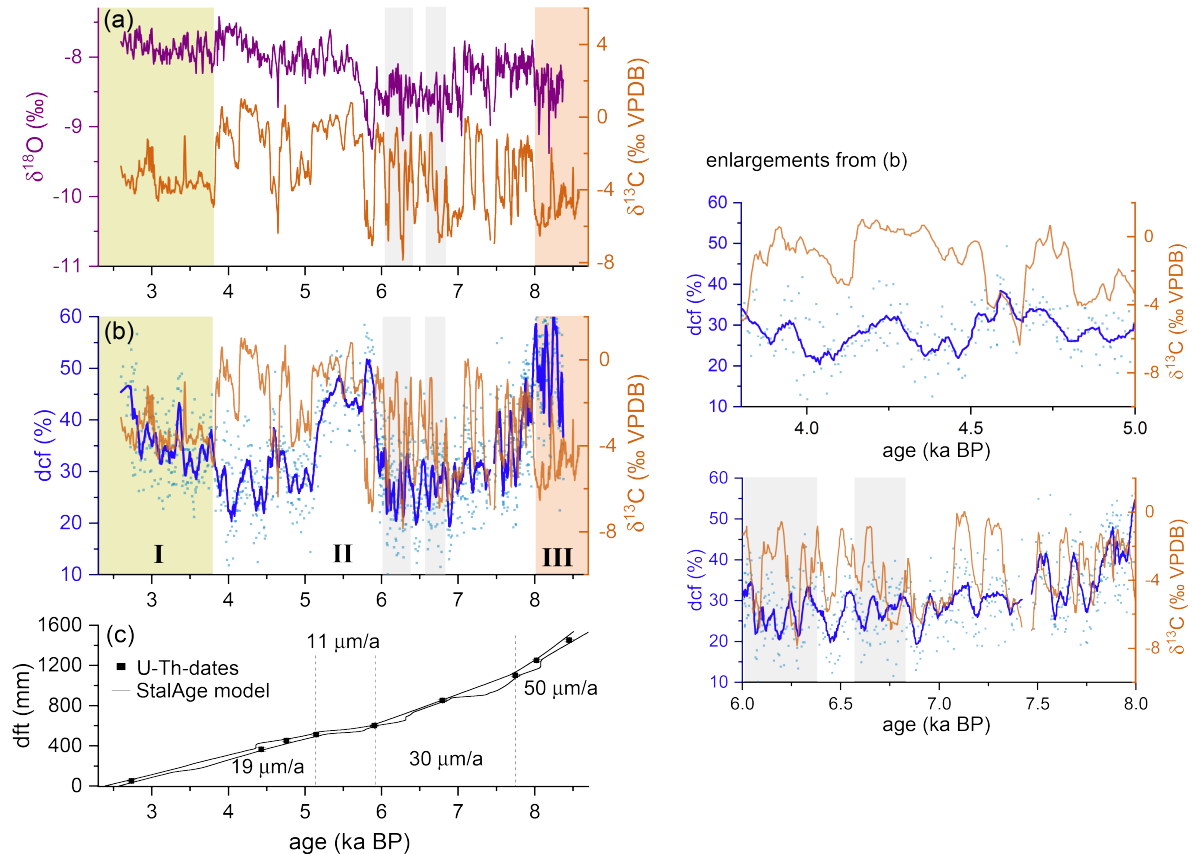
215 The interpretation of the results on C isotopes in SPA 127 will be divided in three sections that correspond to three
 216 sections identified on the speleothem based on their $\delta^{13}C$ characteristics, i.e., two periods of comparably stable
 217 $\delta^{13}C$ before 8 ka BP and after 3.5 ka BP and the interval in between with large and rapid fluctuations.

218 5.1 Old section of SPA 127 (8.5-8.0 ka BP)

219 In the oldest part of SPA 127, the dcf is comparably high (~60%), while $\delta^{13}C$ is relatively depleted with values
 220 lower than -5‰ on average. Although the reservoir effect is extremely high, in principle the obtained C-isotope
 221 composition can be explained without a major contribution of pyrite oxidation. The relatively low $\delta^{13}C$ value of -

222 5‰ actually contradicts this mode of host rock dissolution but is in line with a sparse C3 vegetation ($\delta^{13}\text{C} \approx -25\text{‰}$)
223 above the cave and host rock dissolution under nearly closed conditions (compare Fig. 4 c and d). The
224 stoichiometry of CaCO_3 dissolution by carbonic acid predicts that only about half of the C in the solution is derived
225 from the host rock under nearly completely closed conditions. Given that the Jurassic host rock is devoid of ^{14}C ,
226 the biogenic component must be older than the contemporaneous atmosphere to allow dcf values greater than 50%.
227 Thus, in addition to the atmospheric radiocarbon contribution from living vegetation, an “old” OM source, which
228 respire radiocarbon-depleted CO_2 , is required to explain the depleted $\delta^{13}\text{C}$ values and elevated dcf. Such “old”
229 OM is also argued to have contributed to the radiocarbon reservoir effect of Moomi Cave (Socotra Island) during
230 the last glacial period (Therre et al., 2020). Observations from other cave and karst systems also point to important
231 C pools deep in the vadose karst, e.g., (Benavente et al., 2010; Bergel et al., 2017; Breecker et al., 2012).
232 Nevertheless, in a sparsely vegetated high elevation region this is the first finding of this kind.

233 The speleothem growth phase prior to 8.0 ka coincides with the early Holocene thermal maximum, which is also
234 reflected by the depleted $\delta^{18}\text{O}$ values hinting towards higher temperatures (Fohlmeister et al., 2013; Mangini et
235 al., 2005). Warmer periods likely favor microbial decomposition of, e.g., OM present in the epikarst below the soil
236 zone, which leads to an increase in pCO_2 and, hence, more acidic water. In turn, more CaCO_3 can be dissolved
237 giving rise to higher speleothem growth rates, which is indeed observed in this period (Fig. 3, orange shaded area).
238 Thus, growth rate and the C-isotope composition of stalagmite SPA 127 are in agreement with the presence of a
239 deep OM reservoir in the karst system above the cave.



240
 241 *Figure 3: $\delta^{18}\text{O}$ represented by the purple line (Fohlmeister et al., 2013) compared to $\delta^{13}\text{C}$ (orange line) and (b) dcf (light blue*
 242 *dots) with a 21 point SG filter (dark blue line) plotted against age and compared to $\delta^{13}\text{C}$. The yellow, white and orange shaded*
 243 *areas represent phases with distinct stable isotope characteristics. Roman numbers indicate the three subsections discussed in*
 244 *the text. Light grey shaded areas mark regions where the SG filter was determined with lower confidence. Enlargements of this*
 245 *graph are shown in the right panel. (c) Growth history of SPA 127 obtained by StalAge applied to dated depths (black squares,*
 246 *errors are smaller than the symbol size). Numbers represent average growth rates of the individual sections.*

247 5.2 Rapid changes in dcf and stable C isotopes (8.0 to 3.8 ka BP)

248 The growth rate was reduced in this period compared to the previous one (Fig. 3 c). This either suggests that
 249 meteoric precipitation or the amount of soil-derived C were reduced, both resulting in a smaller amount of
 250 dissolved carbonate transported to the cave. The low $\delta^{13}\text{C}$ values of the first growth period were superseded by
 251 rapid and very large variations of $\delta^{13}\text{C}$. This pattern is complex and its interpretation is difficult, as this behavior
 252 has not been observed elsewhere. Processes in the soil and karst as well as in-cave processes must be considered.
 253 High-resolution LA-AMS ^{14}C measurements in conjunction with O isotope data and growth rate changes, however,
 254 greatly assist in disentangling the driving mechanism(s) for these $\delta^{13}\text{C}$ variations. The dcf between 8.0 and 3.8
 255 ka BP is generally lower than in the older section. This means that either the aged OM in the karst was depleted
 256 or its degradation was reduced, possibly due to a reduction in meteoric precipitation (as deduced from growth rate
 257 reduction). Both reasons, less meteoric precipitation and a depleted deep OM pool, would well explain the
 258 observed reduction in growth rate. The only speleothem C sources available in this period were consequently the
 259 close-to-modern SOM and the radiocarbon-free host rock.

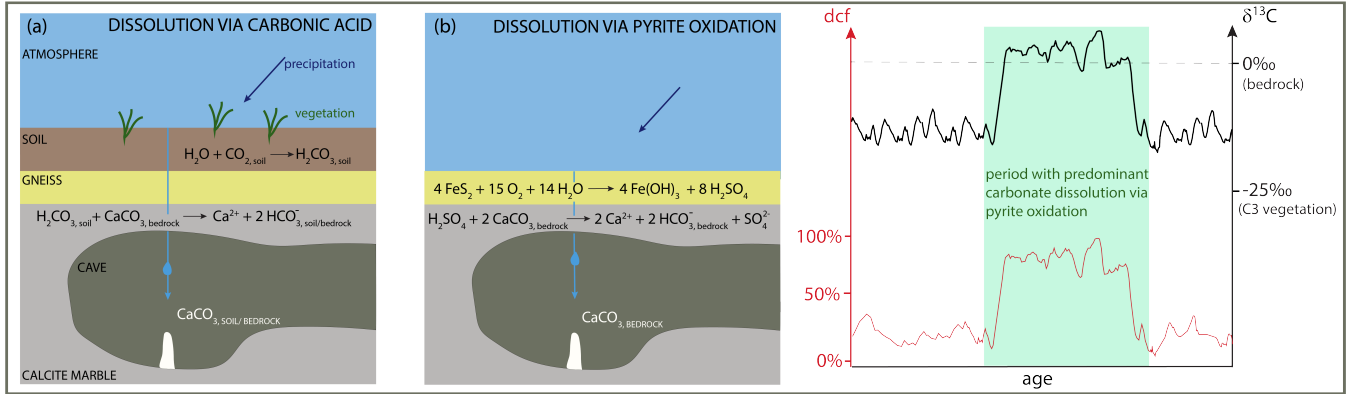
260 The dcf record shows a strong and rapid increase around 6 ka and a rapid decrease back to pre-6 ka levels at around
261 5 ka (Fig. 3 b). The increase in dcf occurs at the same time as a significant decrease in $\delta^{18}\text{O}$, but dcf remains
262 elevated when $\delta^{18}\text{O}$ jumps back again shortly after. Instead, the decrease in dcf at 5 ka occurs contemporaneously
263 with a $\delta^{13}\text{C}$ decrease after $\delta^{13}\text{C}$ values remained at elevated values for nearly a millennium. The reason for such a
264 behavior of the dcf remains elusive. In this section, we focus on the cause of the large and rapid jumps in $\delta^{13}\text{C}$ by
265 proposing two hypotheses.

266 **Hypothesis 1:** Processes above the cave, i.e. different carbonate dissolution processes, cause the rapid switching

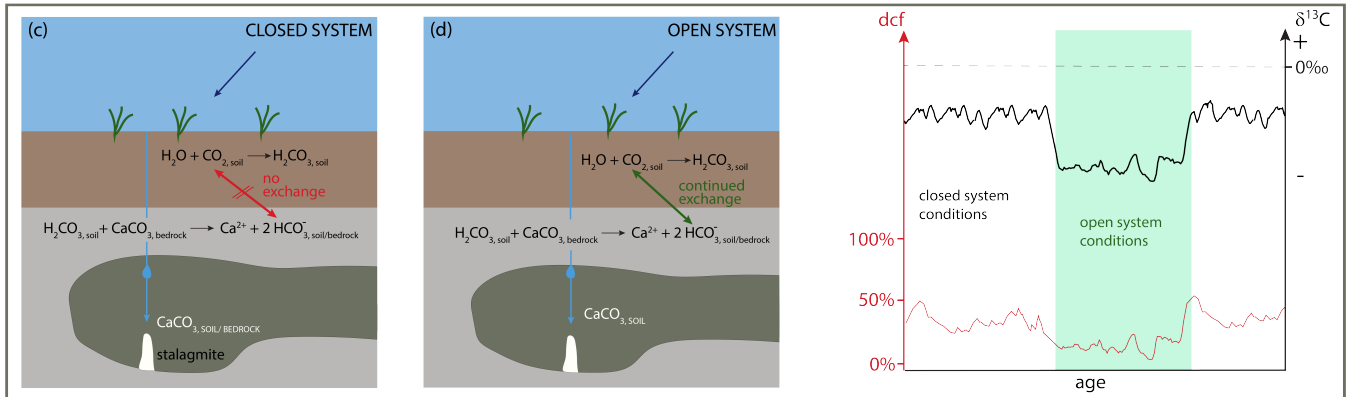
267 Two different processes may have caused carbonate dissolution at Spannagel cave in this period. The first involves
268 soil CO_2 -derived carbonic acid (from root respiration and microbial decomposition of SOM) while the second
269 process operates via sulfuric acid formed by pyrite oxidation (compare Fig. 4 a and b). During times when the first
270 process dominates, the stable carbon isotopic composition of stalagmites is strongly influenced by C from the soil
271 shifting $\delta^{13}\text{C}$ towards more negative values. At the same time, the dcf is expected to be relatively low (at least
272 <50%) as the comparably ^{14}C -rich soil C contributes significantly to the signal. In contrast, pyrite oxidation leads
273 to more positive $\delta^{13}\text{C}$ values in the stalagmite corresponding to the $\delta^{13}\text{C}$ composition of the host rock, as the $\delta^{13}\text{C}$ -
274 depleted biogenic source contributes little or even no C (Bajo et al., 2017; Spötl et al., 2016). Under these
275 conditions, the dcf should increase to values close to 100% if the comparably modern soil contribution is absent.
276 If the observed $\delta^{13}\text{C}$ variations are caused by rapid alternation between both processes, a positive correlation
277 between $\delta^{13}\text{C}$ and the dcf has to be expected, with extreme values in the dcf as outlined above. However, no
278 significant long-term positive correlation for the two data series, i.e. $\delta^{13}\text{C}$ and dcf, is observed (Fig. S10) and
279 extreme dcf values are not observed. A robust comparison of both data sets is impeded because of the different
280 spatial offset of the two measurement tracks from the growth axis. The radiocarbon track is located ca. 5 mm
281 further from the central growth axis than the stable isotope track (Fig. 2). Growth layers cannot be identified, but
282 the small stalagmite diameter suggests steeply dipping layers resulting in an apparent shift of the dcf towards older
283 ages relative to $\delta^{13}\text{C}$. Indeed, such a delay is observable when comparing details in the two data series (Fig. 3 b).
284 Considering the potential offset between the two records (see section 3), a high degree of similarity between main
285 features in $\delta^{13}\text{C}$ and dcf are observable for the middle period, especially between 8 and 6 ka and also partly between
286 5 and 3.8 ka BP. Those phases are interrupted by the interval of the previously described strong increase in dcf.

287 The large swings in $\delta^{13}\text{C}$ suggest frequent switches between the carbonate dissolution mechanism from carbonic
288 acid dissolution to pyrite oxidation. However, this is expected to be accompanied by an increase of the dcf to 100%
289 because of the diminishing ^{14}C -rich soil signature, which, however, is not observed. Generally, the dcf is even
290 smaller than in the youngest and oldest sections of the stalagmite, i.e. after 3.8 ka and before 8 ka BP. Changes
291 between open and closed carbonate dissolution regimes are expected to result in a positive relationship between
292 the dcf and $\delta^{13}\text{C}$, which is observed in SPA 127. However, the magnitude of $\delta^{13}\text{C}$ variations is too large to be
293 explained by a change of the dissolution regimes even when considering the extreme switch from completely open
294 to completely closed (Hendy, 1971; Fohlmeister et al., 2011). Thus, additional processes in the cave most likely
295 caused this unusual behavior and the high-magnitude and high-frequency $\delta^{13}\text{C}$ variations.

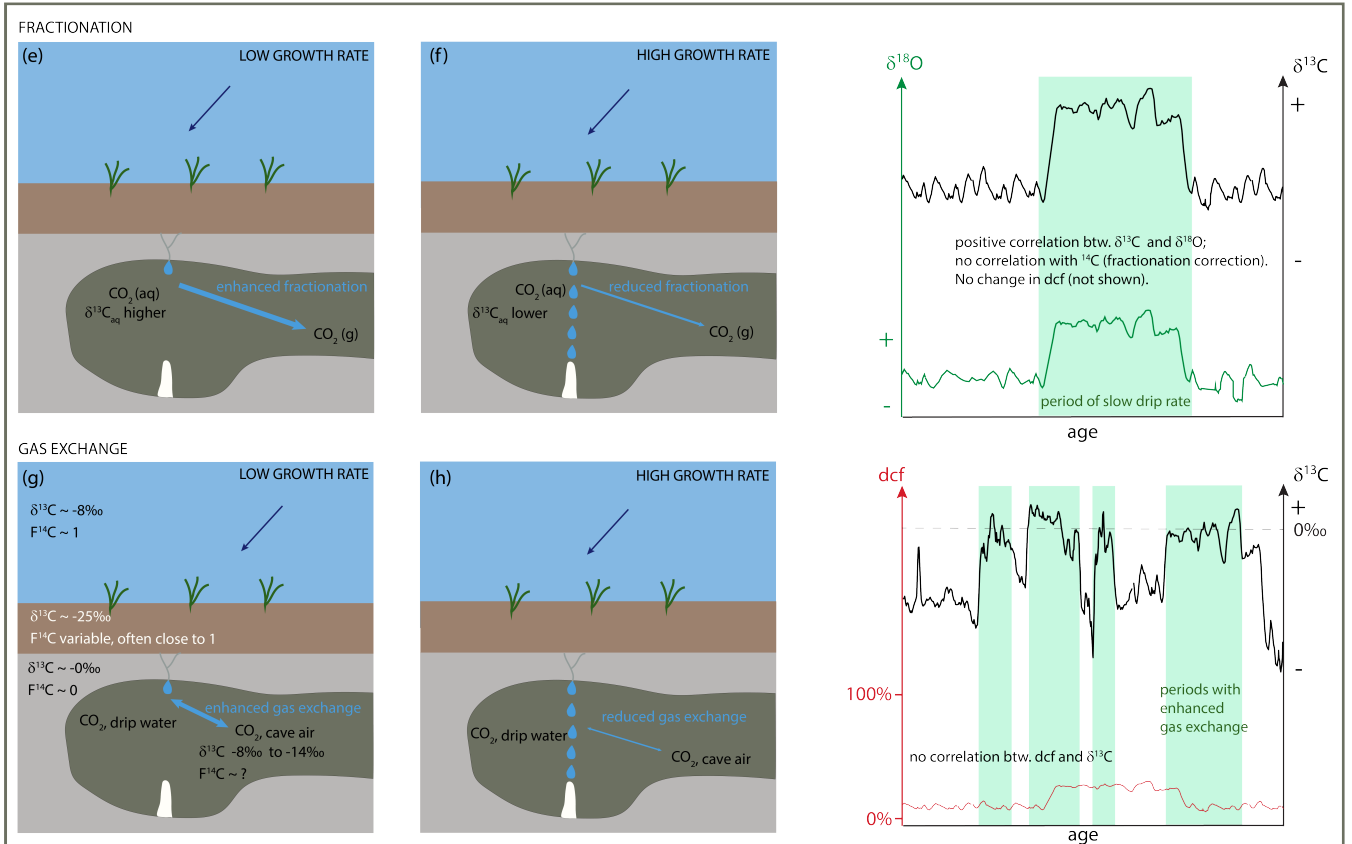
CARBONATE DISSOLUTION MECHANISM ALTERNATING BETWEEN SOIL CO₂ AND SULFIDE OXIDATION



CARBONATE DISSOLUTION MECHANISM: OPEN vs. CLOSED



PROCESSES IN CAVE: FRACTIONATION



296

297 Fig. 4 Overview of different processes that can influence F¹⁴C and δ¹³C in speleothems. For details see text.

298 • **Hypothesis 2:** Processes in the cave cause the rapid switching

299 A major factor influencing the carbon isotope composition of stalagmites are fractionation processes (compare
300 Fig. 4 e and f), which occur during degassing of CO₂ and precipitation of CaCO₃ from the solution. Fast dripping
301 results in fast growth and leaves less time for fractionation or C isotope exchange (compare Fig. 4 g and h) and
302 vice versa (e.g., Fohlmeister et al., 2018; Scholz et al., 2009). In addition, the difference in pCO₂ between water
303 and cave-air CO₂ can also influence isotope fractionation and C exchange processes. In the middle part of SPA
304 127, the average growth rate decreased to $\leq 30 \mu\text{m/a}$, which is significantly lower than in the oldest section
305 ($50 \mu\text{m/a}$). As discussed earlier, the reduction in growth rate might have been partly induced by reduced meteoric
306 precipitation resulting in slower drip rates or by reduced soil or karst CO₂ concentrations leading to less dissolved
307 host rock CaCO₃. In addition, a lower or absent contribution of an “old” OM reservoir in the karst would have led
308 to a lower pCO₂ difference between the CO₂ concentration in the drip water and cave air, which favors an increase
309 in $\delta^{13}\text{C}$ through C isotope exchange processes in the cave. We hypothesize that the rapid changes in $\delta^{13}\text{C}$ might
310 correlate with short-term changes in growth rate, which cannot be resolved by the available U-Th chronology,
311 enabling or disabling isotope fractionation and C exchange between cave air CO₂ and DIC in drip water that are
312 described in the following two paragraphs.

313 (i) Changes in isotope fractionation effects

314 During periods of slow growth, fractionation processes can significantly alter the isotopic composition of the
315 stalagmite. During CO₂ degassing from the drip water, the lighter molecules are preferentially transferred
316 into the gas phase resulting in a solution enriched in heavy isotopes. Indeed, recent experiments (Fahrni et
317 al., 2017) support earlier findings that fractionation of radiocarbon relative to ¹²C is about twice as large as
318 for ¹³C relative to ¹²C (Stuiver and Robinson, 1974). However, as radiocarbon measurements are corrected
319 for fractionation effects via $\delta^{13}\text{C}$ values, it is impossible to detect a potential correlation between the two
320 isotopes due to fractionation effects. However, potential fractionation affecting $\delta^{13}\text{C}$ also influences $\delta^{18}\text{O}$ and
321 can be confirmed by a positive correlation between stable C isotopes and O isotopes, e.g. (Dreybrodt, 2008;
322 Polag et al., 2010). Applying a running correlation coefficient between $\delta^{13}\text{C}$ and $\delta^{18}\text{O}$ is a powerful tool to
323 detect fractionation changes through time (Fohlmeister et al., 2017). 11-point running correlation coefficients
324 calculated for the two time series of SPA 127 show no stalagmite sections with a high correlation coefficient,
325 but vary without any obvious pattern between -1 and +1 (compare Fig. S10, bottom panel). Thus,
326 fractionation was most likely not the main process causing the large variations in $\delta^{13}\text{C}$, but may have played
327 a minor role during some periods.

328 (ii) Prior calcite precipitation (PCP)

329 PCP can have an effect on $\delta^{13}\text{C}$, even a large ones as observed for our stalagmite. While this would not have
330 an effect on ¹⁴C, we would expect that $\delta^{18}\text{O}$ should show a similar behavior, which is not the case (Fig. 3 a).
331 Thus, we can safely assume, that PCP is not responsible for the rapid changes observed in SPA 127.

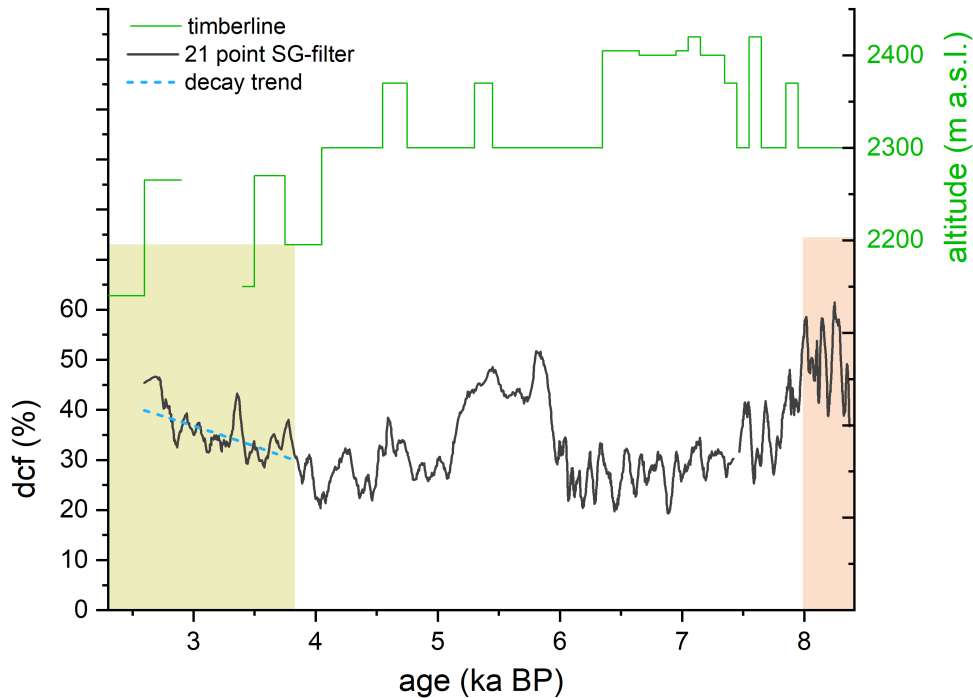
332 C exchange between cave air CO₂ and DIC in drip water. Another process that is a potential candidate for
333 causing the behavior observed in SPA 127 in this interval is the C isotope exchange between CO₂ of the cave
334 air and C dissolved in the drip water. The C exchange between cave air CO₂ and DIC in drip water may be
335 the dominant process if the stalagmite growth rate is sufficiently low and when drip interval is long, meaning
336 that 95% of the CaCO₃ precipitated either via PCP or on the stalagmite (Guo, 2020), and/or the differences
337 between the pCO₂ of the water and cave air is small (Hendy, 1971; Scholz et al., 2009). In this case, the C

338 isotopic composition of the drip water when reaching the top of the stalagmite depends mainly on the initial
339 $\delta^{13}\text{C}$ of drip water and on the degree of C isotope exchange with the cave atmosphere. Spannagel Cave is
340 well ventilated throughout the year with cave air $\delta^{13}\text{C}$ values of -10 to -11‰ (Tochterle et al., 2017), which
341 is significantly lower than that of the atmosphere, i.e. approximately -8‰ (Keeling et al., 2010). These more
342 negative values are a hint towards a contribution from soil air. The following assumptions were made: the
343 $\delta^{13}\text{C}$ of drip water is composed of two biogenic C sources ($\delta^{13}\text{C} \sim -25\text{‰}$) and host rock ($\delta^{13}\text{C} \sim +2.8\text{‰}$) and
344 about 20 - 30% are derived from the host rock (based on the dcf in this interval). Accounting for about 10‰
345 to 11‰ fractionation between soil gas CO_2 and HCO_3^- during the transition of soil gas CO_2 to dissolved
346 inorganic carbon (DIC), the initial drip water, which was feeding the stalagmite, had a $\delta^{13}\text{C}$ value between -
347 11.5 and -9‰ (Mook et al., 1974). Considering Rayleigh fractionation effects in the cave, carbonate $\delta^{13}\text{C}$
348 values of -8‰ appear feasible (Scholz et al., 2009, Deininger et al., 2012) without any exchange of C isotopes.
349 C isotope exchange processes lead to water significantly enriched in ^{13}C . When cave air with $\delta^{13}\text{C}$ values
350 around -11‰ exchanges with drip water, the C isotopic composition of the water will increase, as the
351 transition of gaseous CO_2 to HCO_3^- involves a fractionation of about +10 to +11‰ at temperatures between
352 0 and 5°C (Mook et al., 1974). Thus, drip water in C isotopic equilibrium with cave air CO_2 , which is the
353 most extreme case, should have $\delta^{13}\text{C}$ values of -1 to 0‰. Precipitation of CaCO_3 from such water would
354 result in $\delta^{13}\text{C}$ values of around 0 to +1‰ as observed for some short intervals.

355 Similar considerations can be applied to radiocarbon. If the cave ventilation is sluggish, F^{14}C in the cave air
356 will deviate from atmospheric values (i.e. $\text{F}^{14}\text{C}_{\text{atm}} \approx 1$) as it is influenced by other sources, such as soil air or
357 CO_2 degassed from drip water, which both are depleted with respect to atmospheric values. In a recent study,
358 cave air has been shown to be depleted in radiocarbon with values as low as $\text{F}^{14}\text{C} \approx 0.6$ (Minami et al., 2015).
359 When the cave ventilation is not effectively changing the depleted radiocarbon towards more atmospheric
360 values, C isotope exchange processes are not detectable using ^{14}C in speleothems. As isotopic fractionation
361 is not important for radiocarbon (as explained above), C isotope exchange of DIC with cave air, which both
362 have a similar radiocarbon content, would have no effect on the ^{14}C signal of the precipitated calcite.

363 5.3 Interpretation of dcf and $\delta^{13}\text{C}$ in the youngest section of SPA 127 (3.8 to 2.5 ka BP)

364 In the youngest section of this stalagmite a behavior similar to the oldest section with respect to $\delta^{13}\text{C}$ and
365 radiocarbon content is observed. From approximately 3.8 ka BP onward, the dcf increases slowly from about 20%
366 to 50%. Correspondingly, $\delta^{13}\text{C}$ shows a lower variability than in the middle part with mean $\delta^{13}\text{C}$ values of -3‰ to
367 -4‰, which is also comparable to the behavior observed for the interval > 8 ka BP. As $\delta^{13}\text{C}$ does not show any
368 long-term trend as observed for the reservoir effect, we rule out a change to more closed carbonate dissolution
369 conditions driving the increase in dcf. The only explanation that can lead to such an increase is an “old” C reservoir.
370 We propose that climatic conditions changed such that this “old” OM pool in the karst, which was decoupled from
371 the atmosphere, has become the main OM derived CO_2 source. This CO_2 resulted in acidification in a comparable
372 way as soil CO_2 enhancing carbonate dissolution and ultimately contributed to stalagmite CaCO_3 . The isotopic ^{14}C
373 imprint, however, is significantly different to soil CO_2 causing the observed increase in dcf. Between
374 approximately 8 and 6 ka BP the Alps experienced a warmer climate than today (Ivy-Ochs et al., 2009; Nicolussi
375 et al., 2005). A study conducted by Nicolussi et al. (2005) in the Kauner valley, situated approximately 70 km west
376 of Spannagel Cave, showed that the timberline was significantly higher during that period (Fig. 5) supporting a
377 warmer climate. Between 6 and 4 ka BP the timberline was comparable to the present-day situation.



378

379 *Figure 5: Comparison of the dcf in stalagmite SPA 127 with the elevation of the timberline reconstructed for the Kauner*
 380 *valley 70 km west of Spannagel Cave (green line, after Nicolussi et al. (2005)) with the dcf. Around 4 ka BP the timberline*
 381 *started to decline which is concurrent with an increase in dcf, i.e., a decrease in initial ^{14}C . This decrease closely follows a*
 382 *radiocarbon decay trend (dashed blue line). Green and red areas mark the three different time periods as indicated in Fig. 4.*

383 It is expected that with the lowering of the timberline after ~ 4 ka the vegetation density decreased as well, which
 384 should be reflected in the speleothem- $\delta^{13}\text{C}$ values. This, however, is not the case during this period pointing
 385 towards a relatively stable contribution of soil-derived CO_2 . Possibly, a certain proportion of plants that grew
 386 during the early to mid-Holocene warm epoch died and the corresponding OM located in the deeper vadose zone
 387 was initially stabilized due to reduced meteoric precipitation and later became mobilized due to enhanced microbial
 388 activity. Considering the low mean annual temperatures at this high-alpine site, decomposition processes are most
 389 likely slow, allowing OM to age during decomposition as indicated in a recent study by Shi et al. (2020). The
 390 radiocarbon composition of the ageing SOM will closely follow a radiocarbon-specific exponential decay and is
 391 responsible for the depleted radiocarbon concentration in soil gas CO_2 . Depending on the contribution of root-
 392 respired CO_2 of Alpine plants compared to the decomposed CO_2 from dead OM, the dcf will closely follow an
 393 exponential decay, resembling that of the radiocarbon decay and thus would contribute to the observed increase of
 394 the dcf. The closer the observed increase in the dcf follows that of a radiocarbon decay trajectory, the larger the
 395 contribution of CO_2 from the ageing SOM reservoir in relation to root-respired CO_2 . Based on the observed rate of
 396 increase in dcf, which compares well with the radiocarbon decay trend (blue dashed line in Fig. 5), we suggest that
 397 the majority of DIC that contributed to the speleothem CaCO_3 had its origin in aged soil OM.

398 6 Conclusion

399 Combined stable carbon isotope and radiocarbon analyses of stalagmite SPA 127 provide a comprehensive picture
 400 of the carbon dynamics at Spannagel Cave. With the novel LA-AMS technique, a highly spatially resolved ^{14}C
 401 time series allows unprecedented insights into processes in this high-alpine karst system. Care has to be taken
 402 when applying LA-AMS to stalagmites as epoxy resin used in sample preparation leads to distorted results.

403 Results from this study allow to distinguish three intervals with different carbon dynamics:

404 (i) The interval before 8 ka BP is characterized by generally low and stable $\delta^{13}\text{C}$ values combined with a
405 comparably high dcf (>50%) pointing towards the existence of an “old” OM reservoir in the epikarst.
406 CO_2 emanating from this presaged C pool provides additional carbonic acid potentially enhancing
407 bedrock dissolution.

408 (ii) The interval between 8 and 3.8 ka BP is characterized by a strong variability in $\delta^{13}\text{C}$ with a generally
409 lower dcf suggesting that the “old” OM reservoir in the karst had either been exhausted or stabilized (less
410 production to aged respired soil/karst CO_2) possibly due to reduced meteoric precipitation. This is
411 supported by a lower stalagmite growth rate in this period. C exchange between cave air CO_2 and DIC in
412 drip water is the most likely explanation for the strong $\delta^{13}\text{C}$ variability, as (i) bedrock dissolution
413 mechanisms, i.e. pyrite oxidation vs. carbonic acid dissolution, are not supported by the magnitude of
414 changes in dcf and stable C, even though the temporal coherence indicates that some of the $\delta^{13}\text{C}$ variations
415 might be explained by the bedrock dissolution mode (open vs. closed carbonate dissolution) and, (ii)
416 fractionation processes in the cave cannot explain the large shifts as no correlation between $\delta^{18}\text{O}$ and $\delta^{13}\text{C}$
417 is observed.

418 (iii) In the interval between 3.8 and 2.4 ka BP the comparably more stable $\delta^{13}\text{C}$ signature combined with an
419 increasing dcf hints towards a contribution from an ageing OM reservoir in the karst similar to the period
420 > 8 ka BP. This OM reservoir contributed to the stalagmite growth in this period due to warmer climatic
421 conditions. While the contribution of “old” OM in the oldest growth phase was stable, the youngest
422 section indicates an ageing of this reservoir.

423 **Author contribution**

424 CW, JF and CS conceptualized the content of this manuscript. CW, MW, BH carried LA-AMS measurements out,
425 CS conducted stable carbon isotope analyses. MW and LW developed the data reduction strategy. JF, CW and TE
426 interpreted the data and compared them to published records. CW prepared the manuscript with contributions from
427 all co-authors.

428 **Competing interests**

429 The authors declare that they have no conflict of interest.

430 **Acknowledgements**

431 JF acknowledge support from DFG grants FO 809/2-1 and FO 809/4-1. MW was supported by ETH Research
432 Grant ETH-03 18-2. FTIR analyses were performed by Laura Hendriks. We also thank the two reviewers who
433 helped improving this manuscript.

434

435 References

- 436 Bajo, P., Borsato, A., Drysdale, R., Hua, Q., Frisia, S., Zanchetta, G., Hellstrom, J., and Woodhead, J.:
437 Stalagmite carbon isotopes and dead carbon proportion (DCP) in a near-closed-system situation: An
438 interplay between sulphuric and carbonic acid dissolution, *Geochimica Et Cosmochimica Acta*, 210,
439 208-227, 2017.
- 440 Bar-Matthews, M., Ayalon, A., Kaufman, A., and Wasserburg, G. J.: The Eastern Mediterranean
441 paleoclimate as a reflection of regional events: Soreq cave, Israel, *Earth and Planetary Science Letters*,
442 166, 85-95, 1999.
- 443 Benavente, J., Vadillo, I., Carrasco, F., Soler, A., Linan, C., and Moral, F.: Air Carbon Dioxide Contents in
444 the Vadose Zone of a Mediterranean Karst, *Vadose Zone Journal*, 9, 126-136, 2010.
- 445 Bergel, S. J., Carlson, P. E., Larson, T. E., Wood, C. T., Johnson, K. R., Banner, J. L., and Breecker, D. O.:
446 Constraining the subsoil carbon source to cave-air CO₂ and speleothem calcite in central Texas,
447 *Geochimica Et Cosmochimica Acta*, 217, 112-127, 2017.
- 448 Breecker, D. O., Payne, A. E., Quade, J., Banner, J. L., Ball, C. E., Meyer, K. W., and Cowan, B. D.: The
449 sources and sinks of CO₂ in caves under mixed woodland and grassland vegetation, *Geochimica Et*
450 *Cosmochimica Acta*, 96, 230-246, 2012.
- 451 Cerling, T. E.: The Stable Isotopic Composition of Modern Soil Carbonate and Its Relationship to
452 Climate, *Earth and Planetary Science Letters*, 71, 229-240, 1984.
- 453 Cheng, H., Edwards, R. L., Shen, C.-C., Polyak, V. J., Asmerom, Y., Woodhead, J., Hellstrom, J., Wang, Y.,
454 Kong, X., and Spötl, C.: Improvements in ²³⁰Th dating, ²³⁰Th and ²³⁴U half-life values, and U-Th
455 isotopic measurements by multi-collector inductively coupled plasma mass spectrometry, *Earth and*
456 *Planetary Science Letters*, 371, 82-91, 2013.
- 457 Cheng, H., Edwards, R. L., Sinha, A., Spötl, C., Yi, L., Chen, S., Kelly, M., Kathayat, G., Wang, X., Li, X.,
458 Kong, X., Wang, Y., Ning, Y., and Zhang, H.: The Asian monsoon over the past 640,000 years and ice age
459 terminations, *Nature*, 534, 640-646, 2016.
- 460 Denniston, R. F., DuPree, M., Dorale, J. A., Asmerom, Y., Polyak, V. J., and Carpenter, S. J.: Episodes of
461 late Holocene aridity recorded by stalagmites from Devil's Icebox Cave, central Missouri, USA,
462 *Quaternary Research*, 68, 45-52, 2007.
- 463 Dreybrodt, W.: Evolution of the isotopic composition of carbon and oxygen in a calcite precipitating
464 H₂O-CO₂-CaCO₃ solution and the related isotopic composition of calcite in stalagmites, *Geochimica*
465 *et Cosmochimica Acta*, 72, 4712-4724, 2008.
- 466 Fahrni, S. M., Southon, J. R., Santos, G. M., Palstra, S. W., Meijer, H. A., and Xu, X.: Reassessment of the
467 ¹³C/¹²C and ¹⁴C/¹²C isotopic fractionation ratio and its impact on high-precision radiocarbon dating,
468 *Geochimica et Cosmochimica Acta*, 213, 330-345, 2017.
- 469 Fairchild, I. J. and Baker, A.: *Speleothem science: from process to past environments*, John Wiley &
470 Sons, 2012.
- 471 Fairchild, I. J., Smith, C. L., Baker, A., Fuller, L., Spötl, C., Matthey, D., McDermott, F., and Eimp:
472 Modification and preservation of environmental signals in speleothems, *Earth-Science Reviews*, 75,
473 105-153, 2006.
- 474 Fohlmeister, J., Arps, J., Spötl, C., Schroder-Ritzrau, A., Plessen, B., Gunter, C., Frank, N., and Trussel,
475 M.: Carbon and oxygen isotope fractionation in the water-calcite-aragonite system, *Geochimica Et*
476 *Cosmochimica Acta*, 235, 127-139, 2018.
- 477 Fohlmeister, J., Kromer, B., and Mangini, A.: The Influence of Soil Organic Matter Age Spectrum on the
478 Reconstruction of Atmospheric C-14 Levels Via Stalagmites, *Radiocarbon*, 53, 99-115, 2011a.
- 479 Fohlmeister, J., Plessen, B., Dudashvili, A. S., Tjallingii, R., Wolff, C., Gafurov, A., and Cheng, H.: Winter
480 precipitation changes during the Medieval Climate Anomaly and the Little Ice Age in arid Central Asia,
481 *Quaternary Science Reviews*, 178, 24-36, 2017.
- 482 Fohlmeister, J., Scholz, D., Kromer, B., and Mangini, A.: Modelling carbon isotopes of carbonates in
483 cave drip water, *Geochimica Et Cosmochimica Acta*, 75, 5219-5228, 2011b.

484 Fohlmeister, J., Schroder-Ritzrau, A., Spotl, C., Frisia, S., Miorandi, R., Kromer, B., and Mangini, A.: The
485 Influences of Hydrology on the Radiogenic and Stable Carbon Isotope Composition of Cave Drip Water,
486 Grotta Di Ernesto (Italy), *Radiocarbon*, 52, 1529-1544, 2010a.

487 Fohlmeister, J., Schroeder-Ritzrau, A., Spoetl, C., Frisia, S., Miorandi, R., Kromer, B., and Mangini, A.:
488 The influences of hydrology on the radiovenic and stable carbon isotope composition of cave drip
489 water, Grotta die Ernesto (Italy), *Radiocarbon*, 52, 1529-1544, 2010b.

490 Fohlmeister, J., Voarintsoa, N. R. G., Lechleitner, F. A., Boyd, M., Brandtstatter, S., Jacobson, M. J., and
491 Oster, J. L.: Main controls on the stable carbon isotope composition of speleothems, *Geochimica Et*
492 *Cosmochimica Acta*, 279, 67-87, 2020.

493 Fohlmeister, J., Vollweiler, N., Spotl, C., and Mangini, A.: COMNISPA II: Update of a mid-European
494 isotope climate record, 11 ka to present, *Holocene*, 23, 749-754, 2013.

495 Genty, D. and Massault, M.: Bomb C-14 recorded in laminated speleothems: Calculation of dead
496 carbon proportion, *Radiocarbon*, 39, 33-48, 1997.

497 Gray, A. L.: Solid Sample Introduction by Laser Ablation for Inductively Coupled Plasma Source-Mass
498 Spectrometry, *Analyst*, 110, 551-556, 1985.

499 Griffiths, M. L., Fohlmeister, J., Drysdale, R. N., Hua, Q., Johnson, K. R., Hellstrom, J. C., Gagan, M. K.,
500 and Zhao, J. X.: Hydrological control of the dead carbon fraction in a Holocene tropical speleothem,
501 *Quat. Geochronol.*, 14, 81-93, 2012.

502 Guo, W.: Kinetic clumped isotope fractionation in the DIC-H₂O-CO₂ system: Patterns, controls, and
503 implications, *Geochimica et Cosmochimica Acta*, 268, 230-257, 2020.

504 Hendy, C. H.: The isotopic geochemistry of speleothems—I. The calculation of the effects of different
505 modes of formation on the isotopic composition of speleothems and their applicability as
506 palaeoclimatic indicators, *Geochimica et cosmochimica Acta*, 35, 801-824, 1971.

507 Ivy-Ochs, S., Kerschner, H., Maisch, M., Christl, M., Kubik, P. W., and Schluchter, C.: Latest Pleistocene
508 and Holocene glacier variations in the European Alps, *Quaternary Science Reviews*, 28, 2137-2149,
509 2009.

510 Keeling, R., Piper, S., Bollenbacher, A., and Walker, S.: Monthly atmospheric ¹³C/¹²C isotopic ratios
511 for 11 SIO stations, *Trends: a compendium of data on global change*, 2010. 2010.

512 Koch, J. and Gunther, D.: Review of the state-of-the-art of laser ablation inductively coupled plasma
513 mass spectrometry, *Appl Spectrosc*, 65, 155-162, 2011.

514 Kutschera, W.: Applications of accelerator mass spectrometry, *International Journal of Mass*
515 *Spectrometry*, 349, 203-218, 2013.

516 Lachniet, M. S.: Climatic and environmental controls on speleothem oxygen-isotope values,
517 *Quaternary Science Reviews*, 28, 412-432, 2009.

518 Lauritzen, S.-E.: Marble stripe karst of the Scandinavian Caledonides: an end-member in the contact
519 karst spectrum, *Slovenska akademija znanosti in umetnosti*, 2001.

520 Lechleitner, F. A., Baldini, J. U. L., Breitenbach, S. F. M., Fohlmeister, J., McIntyre, C., Goswami, B.,
521 Jamieson, R. A., van der Voort, T. S., Prufer, K., Marwan, N., Culleton, B. J., Kennett, D. J., Asmerom, Y.,
522 Polyak, V., and Eglinton, T. I.: Hydrological and climatological controls on radiocarbon concentrations
523 in a tropical stalagmite, *Geochimica Et Cosmochimica Acta*, 194, 233-252, 2016.

524 Mangini, A., Spötl, C., and Verdes, P.: Reconstruction of temperature in the Central Alps during the
525 past 2000 yr from a $\delta^{18}\text{O}$ stalagmite record, *Earth and Planetary Science Letters*, 235, 741-751, 2005.

526 Matthey, D. P., Atkinson, T. C., Barker, J. A., Fisher, R., Latin, J. P., Durrell, R., and Ainsworth, M.: Carbon
527 dioxide, ground air and carbon cycling in Gibraltar karst, *Geochimica Et Cosmochimica Acta*, 184, 88-
528 113, 2016.

529 Minami, M., Kato, T., Horikawa, K., and Nakamura, T.: Seasonal variations of ¹⁴C and $\delta^{13}\text{C}$ for cave
530 drip waters in Ryugashi Cave, Shizuoka Prefecture, central Japan, *Nuclear Instruments and Methods in*
531 *Physics Research Section B: Beam Interactions with Materials and Atoms*, 362, 202-209, 2015.

532 Mook, W. G., Bommerson, J. C., and Staverman, W. H.: Carbon Isotope Fractionation between
533 Dissolved Bicarbonate and Gaseous Carbon-Dioxide, *Earth and Planetary Science Letters*, 22, 169-176,
534 1974.

535 Moseley, G. E., Spotl, C., Brandstatter, S., Erhardt, T., Luetscher, M., and Edwards, R. L.: NALPS19: sub-
536 orbital-scale climate variability recorded in northern Alpine speleothems during the last glacial period,
537 *Climate of the Past*, 16, 29-50, 2020.

538 Nicolussi, K., Kaufmann, M., Patzelt, G., van der Plicht, J., and Thurner, A.: Holocene tree-line variability
539 in the Kauner Valley, Central Eastern Alps, indicated by dendrochronological analysis of living trees and
540 subfossil logs, *Vegetation History and Archaeobotany*, 14, 221-234, 2005.

541 Noronha, A. L., Johnson, K. R., Hu, C. Y., Ruan, J. Y., Southon, J. R., and Ferguson, J. E.: Assessing
542 influences on speleothem dead carbon variability over the Holocene: Implications for speleothem-
543 based radiocarbon calibration, *Earth and Planetary Science Letters*, 394, 20-29, 2014.

544 Noronha, A. L., Johnson, K. R., Southon, J. R., Hu, C. Y., Ruan, J. Y., and McCabe-Glynn, S.: Radiocarbon
545 evidence for decomposition of aged organic matter in the vadose zone as the main source of
546 speleothem carbon, *Quaternary Science Reviews*, 127, 37-47, 2015.

547 Polag, D., Scholz, D., Mühlinghaus, C., Spotl, C., Schroder-Ritzrau, A., Segl, M., and Mangini, A.: Stable
548 isotope fractionation in speleothems: Laboratory experiments, *Chemical Geology*, 279, 31-39, 2010.

549 Reimer, P. J., Bard, E., Bayliss, A., Beck, J. W., Blackwell, P. G., Ramsey, C. B., Buck, C. E., Cheng, H.,
550 Edwards, R. L., Friedrich, M., Grootes, P. M., Guilderson, T. P., Hafliðason, H., Hajdas, I., Hatté, C.,
551 Heaton, T. J., Hoffmann, D. L., Hogg, A. G., Hughen, K. A., Kaiser, K. F., Kromer, B., Manning, S. W., Niu,
552 M., Reimer, R. W., Richards, D. A., Scott, E. M., Southon, J. R., Staff, R. A., Turney, C. S. M., and van der
553 Plicht, J.: IntCal13 and Marine13 Radiocarbon Age Calibration Curves 0–50,000 Years cal BP,
554 *Radiocarbon*, 55, 1869-1887, 2016.

555 Richards, D. A. and Dorale, J. A.: Uranium-series chronology and environmental applications of
556 speleothems, *Uranium-Series Geochemistry*, 52, 407-460, 2003.

557 Savitzky, A. and Golay, M. J. E.: Smoothing + Differentiation of Data by Simplified Least Squares
558 Procedures, *Analytical Chemistry*, 36, 1627-8, 1964.

559 Scholz, D. and Hoffmann, D.: ²³⁰Th/U-dating of fossil reef corals and speleothems, *Quater. Sci. J.*, 57,
560 52-77, 2008.

561 Scholz, D. and Hoffmann, D. L.: StalAge - An algorithm designed for construction of speleothem age
562 models, *Quat. Geochronol.*, 6, 369-382, 2011.

563 Scholz, D., Mühlinghaus, C., and Mangini, A.: Modelling δ13C and δ18O in the solution layer on
564 stalagmite surfaces, *Geochimica et Cosmochimica Acta*, 73, 2592-2602, 2009.

565 Shi, Z., Allison, S. D., He, Y. J., Levine, P. A., Hoyt, A. M., Beem-Miller, J., Zhu, Q., Wieder, W. R.,
566 Trumbore, S., and Randerson, J. T.: The age distribution of global soil carbon inferred from radiocarbon
567 measurements, *Nat. Geosci.*, 13, 555-+, 2020.

568 Southon, J., Noronha, A. L., Cheng, H., Edwards, R. L., and Wang, Y.: A high-resolution record of
569 atmospheric 14C based on Hulu Cave speleothem H82, *Quaternary Science Reviews*, 33, 32-41, 2012.

570 Spötl, C.: Long-term performance of the Gasbench isotope ratio mass spectrometry system for the
571 stable isotope analysis of carbonate microsamples, *Rapid Communications in Mass Spectrometry*, 25,
572 1683-1685, 2011.

573 Spotl, C., Fairchild, I. J., and Tooth, A. F.: Cave air control on dripwater geochemistry, Obir Caves
574 (Austria): Implications for speleothem deposition in dynamically ventilated caves, *Geochimica Et*
575 *Cosmochimica Acta*, 69, 2451-2468, 2005.

576 Spötl, C., Fohlmeister, J., Cheng, H., and Boch, R.: Modern aragonite formation at near-freezing
577 conditions in an alpine cave, Carnic Alps, Austria, *Chemical Geology*, 435, 60-70, 2016.

578 Spotl, C. and Mangini, A.: Speleothems and paleoglaciers, *Earth and Planetary Science Letters*, 254,
579 323-331, 2007.

580 Spötl, C. and Mangini, A.: Paleohydrology of a high-elevation, glacier influenced karst system in the
581 central alps (Austria), *Austrian Journal of Earth Sciences*, 103, 92-105, 2010.

582 Spötl, C., Mangini, A., Bums, S. J., Frank, N., and Pavuza, R.: Speleothems from the high-alpine
583 Spannagel cave, Zillertal Alps (Austria). In: *Studies of cave sediments*, Springer, 2004.

584 Spötl, C. and Matthey, D.: Stable isotope microsampling of speleothems for palaeoenvironmental
585 studies: A comparison of microdrill, micromill and laser ablation techniques, *Chemical Geology*, 235,
586 48-58, 2006.

587 Stuiver, M. and Polach, H. A.: Reporting of C-14 Data - Discussion, *Radiocarbon*, 19, 355-363, 1977.
588 Stuiver, M. and Robinson, S. W.: University of Washington GEOSECS north Atlantic carbon-14 results,
589 *Earth and Planetary Science Letters*, 23, 87-90, 1974.
590 Therre, S., Fohlmeister, J., Fleitmann, D., Matter, A., Burns, S. J., Arps, J., Schroder-Ritzrau, A., Friedrich,
591 R., and Frank, N.: Climate-induced speleothem radiocarbon variability on Socotra Island from the Last
592 Glacial Maximum to the Younger Dryas, *Climate of the Past*, 16, 409-421, 2020.
593 Tochterle, P., Dublyansky, Y., Stobener, N., Mandic, M., and Spotl, C.: High-resolution isotopic
594 monitoring of cave air CO₂, *Rapid Commun Mass Spectrom*, 31, 895-900, 2017.
595 Trumbore, S.: Age of soil organic matter and soil respiration: Radiocarbon constraints on belowground
596 C dynamics, *Ecological Applications*, 10, 399-411, 2000.
597 Wackerbarth, A., Scholz, D., Fohlmeister, J., and Mangini, A.: Modelling the $\delta^{18}O$ value of cave drip
598 water and speleothem calcite, *Earth and Planetary Science Letters*, 299, 387-397, 2010.
599 Welte, C., Wacker, L., Hattendorf, B., Christl, M., Fohlmeister, J., Breitenbach, S. F., Robinson, L. F.,
600 Andrews, A. H., Freiwald, A., and Farmer, J. R.: Laser Ablation–Accelerator Mass Spectrometry: An
601 Approach for Rapid Radiocarbon Analyses of Carbonate Archives at High Spatial Resolution, *Analytical*
602 *chemistry*, 88, 8570-8576, 2016a.
603 Welte, C., Wacker, L., Hattendorf, B., Christl, M., Koch, J., Synal, H. A., and Gunther, D.: Novel Laser
604 Ablation Sampling Device for the Rapid Radiocarbon Analysis of Carbonate Samples by Accelerator
605 Mass Spectrometry, *Radiocarbon*, 58, 419-435, 2016b.
606 Welte, C., Wacker, L., Hattendorf, B., Christl, M., Koch, J., Yeman, C., Breitenbach, S. F. M., Synal, H. A.,
607 and Gunther, D.: Optimizing the analyte introduction for C-14 laser ablation-AMS, *Journal of Analytical*
608 *Atomic Spectrometry*, 32, 1813-1819, 2017.
609 Yeman, C., Christl, M., Hattendorf, B., Wacker, L., Welte, C., Brehm, N., and Synal, H. A.: Unravelling
610 Quasi-Continuous ¹⁴C Profiles by Laser Ablation AMS, *Radiocarbon*, 62, 453-465, 2019.

611
612